

Chiral symmetry crossover with a linear confining and temperature dependent quark-antiquark potential.

P. Bicudo*

CFTP, Dep. Física, Instituto Superior Técnico, Av. Rovisco Pais, 1049-001 Lisboa, Portugal

Recently we developed a numerical technique to compute chiral symmetry breaking at $T = 0$ with different current quark masses m_0 , including the current quark masses of the six standard flavours u, d, s, c, b, t . We also fitted from Lattice QCD data the quark-antiquark string tension σ dependence on temperature T . We now utilize $\sigma(T)$ to further upgrade the chiral invariant and confinement quark model to finite temperatures $T \neq 0$. We study the quark mass at finite T and obtain the corresponding chiral crossover at $T = T_c$. The quark mass critical curve has a shape similar, but not identical, to the string tension critical curve. In the case of the lightest quarks, the quark mass and the chiral condensate essentially vanish at $T = T_c$, except for the small explicit chiral symmetry breaking m_u and m_d .

I. INTRODUCTION

A. Motivation.

We address the chiral crossover in the quark model perspective. The chiral crossover is a cornerstone to understand the QCD phase diagram [1], for finite T and μ . Notice that, after enormous numerical efforts, the analytic crossover nature of the finite-temperature QCD transition was finally determined by Y. Aoki *et al.* [2, 3], utilizing Lattice QCD and physical quark, and reaching the continuum extrapolation with a finite volume analysis. The QCD phase diagram is extensively researched at the experimental collaborations LHC, RHIC and FAIR. This will help us to further understand how the universe evolves in the Big bang model of the cosmos.

Here we utilize the linear confining potential for the quark-antiquark interaction, in the Coulomb Gauge Chiral Quark Model (CG χ QM), including both confinement and chiral symmetry [4]. While this model, inspired from the framework of Coulomb gauge Hamiltonian formalism is not yet full QCD, it is presently the only model able to include explicitly both the quark-antiquark confining potential and the quark-antiquark vacuum condensation. The CG χ QM is for instance able to address excited hadrons as in Fig. 1, and chiral symmetry at the same token, and it recently led us to suggest that the infrared enhancement of the quark mass can be observed in the excited baryon spectrum at CBELSA and at JLAB [5, 6].

Chiral symmetry breaking has been studied in detail with the CG χ QM in the chiral limit and at vanishing temperature. It is quite well understood how, in the chiral limit of $m_0 = 0$, the quark develops a constituent running mass $m(p)$ function of the momentum p . $m(p)$ is a solution of the mass gap equation (equivalent to the Schwinger-Dyson equation) for the quark, and this is important to understand the spontaneous breaking of

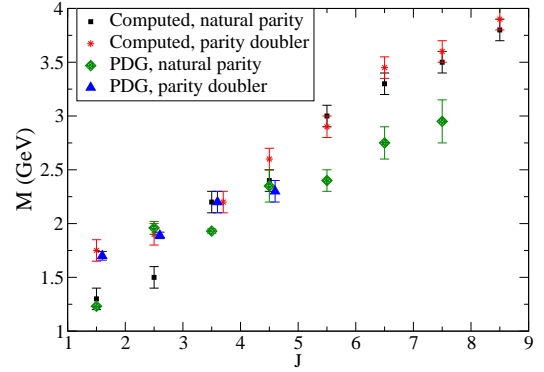


FIG. 1: First calculation of excited baryons with a chiral invariant quark model [5].

chiral symmetry. Although the CG χ QM is adequate to study the QCD phase diagram microscopically, the scientific community is only starting to explore [7–14], the CG χ QM with a finite temperature $T \neq 0$ and with a finite current quark mass $m_0 \neq 0$. Notice that a finite quark mass is not only crucial for the study of the hadron spectra, it is also relevant and for the study the QCD phase diagram. In the phase diagram, a finite current quark mass m_0 affects the position of the critical point between the crossover at low chemical potential μ and the phase transition at higher μ . The present work, not only addresses the QCD phase diagram, but it also constitutes the first step to allow us in the future to extend the computation of any hadron spectrum, say the Fig. 1 computed in reference [5], to finite T .

We now review recent advances, leading to a temperature dependent string tension, and to a more efficient technique to solve the mass gap equation. These advances are applied in Section II, where we derive the mass gap equation at finite Temperature. In Section III we solve the finite T mass gap equation, and compute the running mass $m_T(p)$ to study the chiral crossover. In Section IV we discuss our results and conclude.

*Electronic address: bicudo@ist.utl.pt

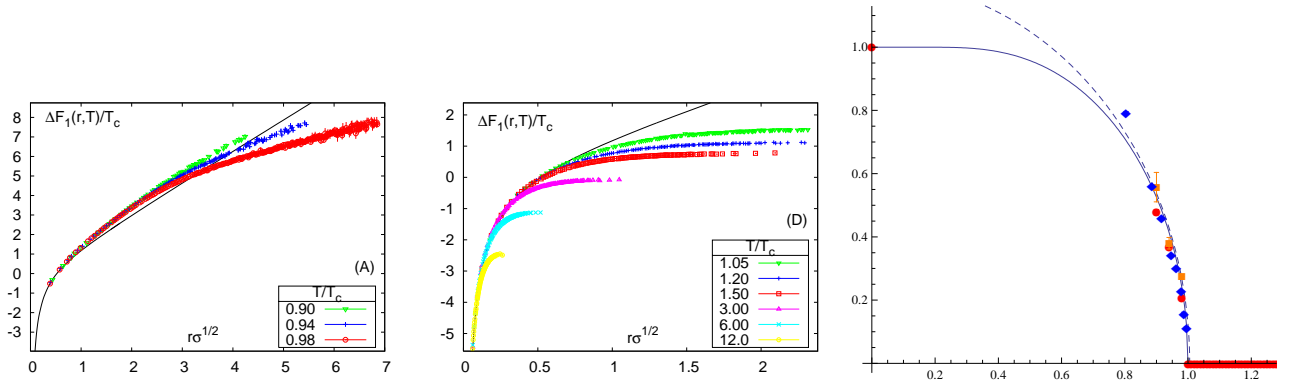


FIG. 2: We compare the $T = 0$ static quark-antiquark potential (solid line, left) to the $T < T_c$ (left) and the $T > T_c$ (centre) Lattice QCD data for the free energy F_1 , thanks to [17–21]Olaf Kaczmarek et al. We also compare (right) the magnetization curve (solid line, right) with the SU(3) string tension critical curve (bullets) computed in Ref. [16]. We show (dashed line, right) the fit $1.21(1 - 0.990(T/T_c)^2)^{1/2}$ used in Ref. [16] to measure the finite string tension at T_c as an evidence for a first order phase transition.

B. The quark-antiquark potential at finite temperature $T \neq 0$.

The most fundamental information for the quark-antiquark interaction in QCD comes from the Wilson loop and from the Polyakov loops in Lattice QCD, providing the confining potential for a static quark-antiquark pair. This potential is consistent with the funnel potential, also utilized in the quark model to describe phenomenologically the quark-antiquark sector of meson spectrum, in particular to describe the linear behaviour of mesonic Regge trajectories. Notice that the short range Coulomb potential could also be included in the interaction, but here we ignore it since it only affects the quark mass through ultraviolet renormalization [15], which is assumed to be already included in the current quark mass. Here we specialize in computing different aspects of chiral symmetry breaking produced by linear confinement $V = \sigma(T)r$.

The finite temperature string tension was computed for the first time by the Bielefeld Group for quenched SU(3) Lattice QCD [16]. The finite temperature static quark-antiquark free and internal energies at some finite temperatures T have also been computed in dynamical SU(3) Lattice QCD, by the Bielefeld for two light flavours $N_f = 2$ [17–21], as depicted in Fig. 2.

Recently we have empirically shown the string tension at finite $T \neq 0$ to be well fitted [22], by a critical curve similar to the spontaneous magnetization of a ferromagnet [23], *i. e.* solution of the algebraic equation,

$$\frac{\sigma(T)}{\sigma(0)} = \tanh \left[\frac{T_c \sigma(T)}{T \sigma(0)} \right]. \quad (1)$$

Although the empirical curve of Eq. (1) corresponds to a second order transition (the solid line at the right of Figure 2), and it is not a crossover as in full QCD, or a first order transition as in pure gauge SU(3) QCD (the

dashed line at the right of Figure 2), the difference between these three scenarios is minute, and the validity of our fit is illustrated in Figure 2. Since the difference of these three scenarios has little effect in the numerics of the finite T mass gap equation, the empirical curve of Eq. (1) provides us with the necessary function $\sigma(T)$ to address confinement at finite temperature.

C. The quark-antiquark potential, the mass gap equation and the Salpeter equation at $T = 0$

To address the light quark sector it is not sufficient to know the static quark-antiquark potential, we also need to know what Dirac vertex to use in the quark-antiquark-interaction. This vertex is necessary to study not only the meson spectrum but also the dynamical spontaneous breaking of chiral symmetry. To determine what vertex to use, we review how the quark-antiquark potential can be approximately derived from QCD, in two different gauges. In Coulomb gauge [24],

$$\nabla \cdot \mathbf{A}(\mathbf{x}, t) = 0 \quad (2)$$

the interaction potential, as derived by Szczepaniak and Swanson [25, 26], is a density-density interaction, with Dirac structure $\gamma^0 \otimes \gamma^0$. Another approximate path from QCD considers the modified coordinate gauge of Balitsky and in the interaction potential for the quark sector, retains the first cumulant order, of two gluons [28–30]. This again results in a simple density-density effective $\gamma^0 \otimes \gamma^0$ confining interaction. Assuming such a Dirac structure, our interaction potential for the quark sector is,

$$V_I = \int d^3x \left[\psi^\dagger(x) (m_0\beta - i\vec{\alpha} \cdot \vec{\nabla}) \psi(x) + \frac{1}{2} \int d^4y \right. \\ \left. \psi^\dagger(\mathbf{x}) \lambda^a \psi(\mathbf{x}) \frac{-3}{16} \sigma(T) |\mathbf{x} - \mathbf{y}| \psi^\dagger(\mathbf{y}) \lambda^b \psi(\mathbf{y}) \right] \quad (3)$$

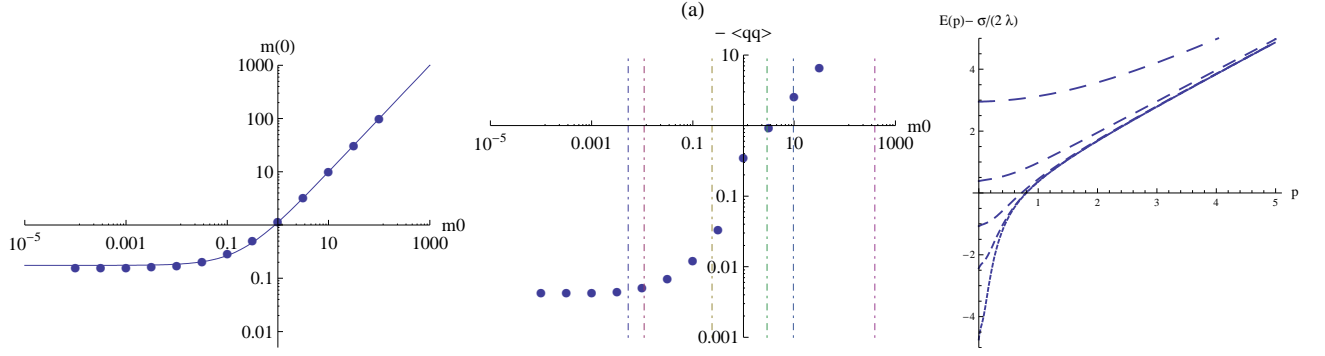


FIG. 3: (left) We plot the solution of the mass gap equation $m(0)$ at $T = 0$, for different values of the current quark mass m_0 in the case where the string tension is $\sigma = 1$, and we also show, with a solid line, the fit with a two-parameter irrational function. (centre) We show a log log plot of minus the regularized quark condensate $-\langle\bar{\psi}\psi\rangle + \langle\bar{\psi}\psi\rangle_0$ as a function of the current quark mass m_0 , with vertical dot-dashed lines representing the current masses of the quarks u, d, s, c, b, t . (right) We represent the regularized quark dispersion relation $E(p) - \frac{\sigma}{2\mu}$ with increasing number of dashes per curve for five different current quark masses m_0 with respective values $10^{-4}, 10^{-1}, 10^{-1/2}, 10^0, 10^{1/2}$. The quark condensate has an inflection point for finite quark masses close to the strange quark mass, and for large masses it rises linearly with m_0 . All results are in dimensionless units of $\sigma = 0.19 \text{ GeV}^2 = 1$.

where the Gell-Mann matrices are denoted λ^a , and the density-density interaction includes just the linear confining potential together with an infrared constant, which may be possibly divergent. While the CG χ QM of Eq. (3) is not exactly equivalent to QCD, we use it as our framework since it includes three crucial aspects of non-perturbative QCD, a chiral invariant quark-antiquark interaction, the cancellation of infrared divergences [31–36], and a quark-antiquark linear potential [25, 37–41]. The mass gap equation and the energy of a quark are determined from the Schwinger-Dyson equation at one loop order using the hamiltonian of Eq. (3). for a recent derivation with all details see [4].

In the limit of vanishing temperature $T = 0$, the interaction in the four momentum of the potential and quark propagator term includes an integral in the energy

$$\int_{-\infty}^{+\infty} \frac{dp^0}{2\pi} \frac{i}{p^0 - E(\mathbf{p}) + i\epsilon} = +\frac{1}{2}, \quad (4)$$

which factorizes trivially from the vector \mathbf{p} momentum integral. Using spherical coordinates, the angular integrals can be performed analytically and finally only an integral in the modulus of the momentum remains to be computed numerically. We arrive at the mass gap equation in two equivalent forms, of a non-linear integral functional equation,

$$0 = pS(p) - m_0C(p) - \frac{\sigma}{p^2} \int_0^\infty \frac{dk}{2\pi} \left[I_A(k, p, \mu) S(k)C(p) - I_B(k, p, \mu) S(p)C(k) \right], \quad (5)$$

and of a minimum equation of the energy density \mathcal{E} ,

$$\mathcal{E} = \frac{-g}{2\pi} \int_0^\infty \frac{dp}{2\pi} \left[2p^3C(p) + 2p^2m_0S(p) + \sigma \times \int_0^\infty \frac{dk}{2\pi} I_A(k, p, \mu) S(k)S(p) + I_B(k, p, \mu) C(p)C(k) \right], \quad (6)$$

where the functions I_B and I_A are angular integrals of the Fourier transform of the potential. In what concerns the one quark energy we get,

$$E(p) = pC(p) + m_0S(p) + \frac{\sigma}{p^2} \int_0^\infty \frac{dk}{2\pi} I_A(k, p, \mu) \times S(k)S(p) + I_B(k, p, \mu) C(p)C(k). \quad (7)$$

We now extend this framework to finite T .

II. IMPLEMENTING FINITE T

A. The quark propagator at finite temperature $T \neq 0$.

We now extend our equal-time density-density confinement to finite temperature. A framework for this extension is the sum in Matsubara frequencies. With the equal time potential in our CG χ QM, the integration in the three-momentum \mathbf{p} and in the energy p^0 are separable, and this is convenient to extend our CG χ QM with a Matsubara.

We first study the wick rotation as a link between Eq. (4) and the Matsubara sum. In the $T = 0$ mass gap equation or Schwinger Dyson equation, we have the Minkowski space integral in p^0 of the quark propagator pole of Eq. (4) and this is equivalent to an integral in p^4 in Euclidian space after a Wick rotation in the Argand space,

$$\int_{-\infty}^{+\infty} \frac{idp^4}{2\pi} \frac{i}{ip^4 - E(\mathbf{p}) + i\epsilon} = +\frac{1}{2}. \quad (8)$$

This simple Wick rotation can be understood considering

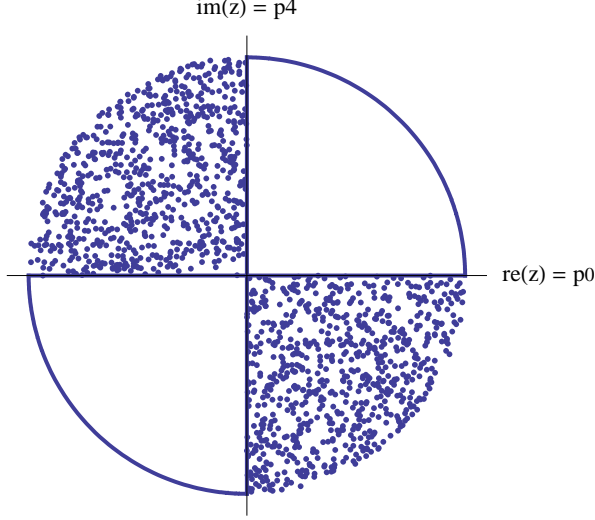


FIG. 4: Artist's view of the Wick rotation. The Wick rotation from a real variable $z = p^0$ to a complex one $z = ip^4$, can be performed without pole corrections, utilizing the depicted contour (solid in the figure), if there are only poles in the second and fourth Argand quadrants (dotted in the figure), and if the integrals in the circular paths of the first and third quadrants cancel in the limit of $|z| \rightarrow \infty$.

the closed contour of Fig. 4

$$\begin{aligned} & \left(\int_{-\infty}^{\infty} + \int_{\infty}^{i\infty} + \int_{i\infty}^{-i\infty} + \int_{-i\infty}^{-\infty} \right) dz f(z) \\ &= \sum_{p_i \in \text{quadrant 1}} \text{Re } f(p_i) + \sum_{p_j \in \text{quadrant 3}} \text{Re } f(p_j). \end{aligned} \quad (9)$$

In the case there are no poles in the first or third quadrant and the circular paths cancel, one just has to replace p^0 by ip^4 since in the real axis the path corresponds to $z = p^0$ and in the imaginary axis the path corresponds to $z = ip^4$.

Notice that the integral in Eq. (8) is only identical to the one in Eq. (4) if the one quark energy $E(p) > 0$. If $E(p) < 0$ the integral of Eq. (8) changes sign, and this is consistent with the pole moving from the fourth quadrant to the third quadrant of the Argand plane. While the integral in Eq. (4) is insensitive to this translation of the pole, the contour of Fig. 4 leads to a pole correction. For simplicity, we choose to work with positive one quark energies only $E(p) > 0$.

In finite temperature T and density ρ , the continuous euclidian space integration of eq. (8) is extended to the sum in Matsubara frequencies,

$$\begin{aligned} & \sum_{n=-\infty}^{+\infty} i kT \frac{i}{i(2n+1)\pi kT - [E(\mathbf{p}) - \mu]} \\ &= \frac{1}{2} \tanh \frac{E(\mathbf{p}) - \mu}{2kT} \end{aligned} \quad (10)$$

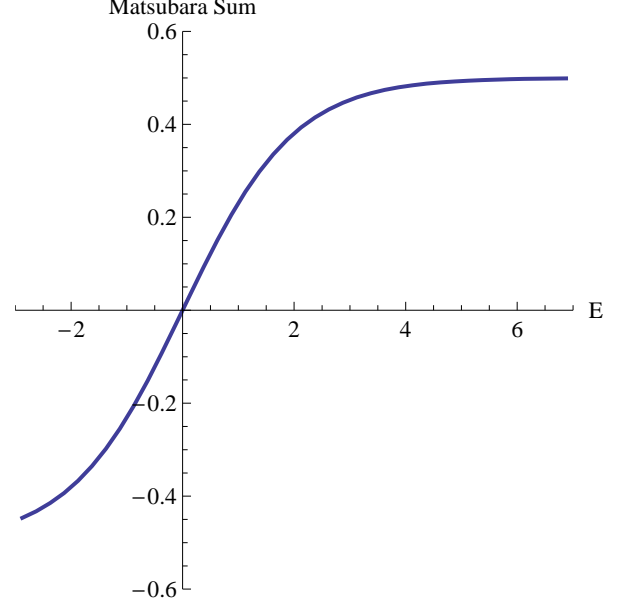


FIG. 5: The sum in Matsubara frequencies of the quark propagator as a function of $\frac{E-\mu}{kT}$, including also energies below the fermi surface. The $T \rightarrow 0$ or $E - \mu \rightarrow \infty$ limit of the sum is $1/2$, as in Eq. (4) or in Eq. (8).

where a chemical potential μ may be included, as a finite density when a Fermi sphere of quarks is present. It is clear that in the vanishing temperature and density $kT \ll E$ limit one gets back the initial Euclidean space integral of eq. (8), when the Matsubara sum approaches the continuum integration with $kT \rightarrow \frac{dP^4}{2\pi}$.

In what concerns the analytical calculations leading to the results in Eqs. (4), (8) and (10), we used the even integral or summation to change the variable to a square, and we respectively used the residue theorem, real and indefinite integrals, and the analytical series summation,

$$\sum_{n=0}^{\infty} \frac{y}{y^2 + (n + 1/2)^2} = \frac{\pi}{2} \tanh \pi y. \quad (11)$$

We verified all three analytical results with numerical integrations or sums. In Fig. (5) we plot the result of Eq. (10) and it is clear that in the vanishing T limit all three analytical results coincide.

B. Infrared regularization of the linear confining potential

Notice that in the case of a linear potential, divergent in the infrared, the Fourier transform needs an infrared regulator λ eventually vanishing. A possible regulariza-

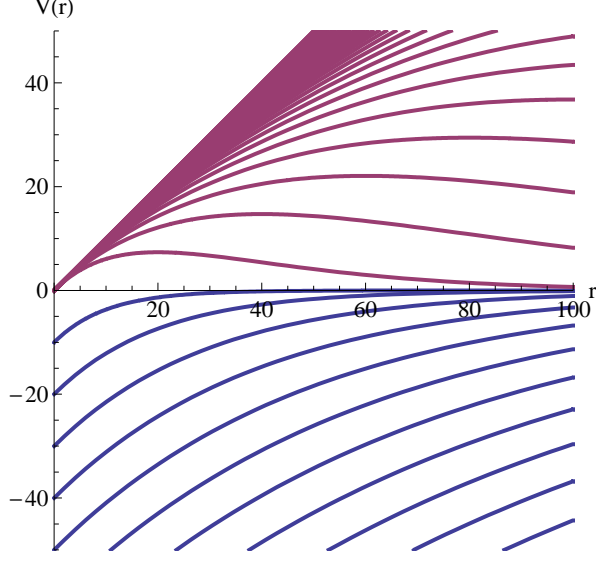


FIG. 6: The linear potential must be regularized for the Fourier Transform, and we show our two different regularizations of Eqs. (12) and (14), both leading to $V(r) \rightarrow \sigma r$ plus a constant when $r \rightarrow 0$. Two successions of curves are plotted, to illustrate the limit of a vanishing infrared regulator $\lambda \rightarrow 0$. The regularization of the negative curves maintains the potential monotonous and $V(\infty) = 0$ but adds an infrared negative constant to the potential. The regularization of the positive curves maintains $V(0) = 0$ but the potential decreases for large r .

tion of the linear potential is,

$$V(r) = -\sigma \frac{e^{-\lambda r}}{\lambda} \simeq -\frac{\sigma}{\lambda} + \sigma r, \quad (12)$$

corresponding to a model of confinement where the quark-antiquark system has an infinite binding energy $\frac{\sigma}{\lambda}$ at the origin $r = 0$, is monotonous and only vanishes at an arbitrarily large distance. This potential has a simple three-dimensional Fourier transform,

$$\begin{aligned} V(k) &= \int_0^\infty dr \frac{4\pi r \sin(kr)}{k} V(r) \\ &= \sigma \frac{-8\pi}{(k^2 + \lambda^2)^2} \end{aligned} \quad (13)$$

and this is the most common form of the linear potential in momentum space utilized in the literature. Notice that this is infrared divergent due to the $-1/\lambda$ infinite binding energy in the limit where the regulator $\lambda \rightarrow 0$. If we want to avoid the infinite binding energy we should use a different regularization of the linear potential, also vanishing when $r \rightarrow \infty$ but not monotonous since it grows linearly at the origin starting with $V(0) = 0$,

$$V(r) = \sigma r e^{-\lambda r} \quad (14)$$

where the Fourier transform,

$$V(k) = \sigma \frac{-8\pi}{(k^2 + \lambda^2)^2} + \sigma \frac{32\pi\lambda^2}{(k^2 + \lambda^2)^3} \quad (15)$$

is such that the integrals in k no longer diverge. For instance,

$$\int_{-\infty}^{+\infty} k^2 dk V(k) = 0 \quad (16)$$

since this is proportional to $V(0) = 0$. The new term in the potential $\frac{32\pi\lambda^2}{(k^2 + \lambda^2)^3}$ is equal to $(2\pi)^3 \delta^3(k)/\lambda$ in the limit $\lambda \rightarrow 0$ and thus the potential in Eq. (15) is infrared finite. Both the potentials in Eqs. (12) and (14) are illustrated in Fig. 6. In the vanishing temperature limit $T = 0$ the different regularizations lead to the same physical results since any constant term in a density-density interaction has no effect in the quark running mass $m(p)$ or in the hadron spectrum [4].

With the potential of Eq. (12) the functions I_B and I_A contributing to the mass gap equation and to the one quark energy are,

$$\begin{aligned} I_A(k, p, \lambda) &= \frac{pk}{(p-k)^2 + \lambda^2} - \frac{pk}{(p+k)^2 + \lambda^2}, \\ I_B(k, p, \lambda) &= \frac{pk}{(p-k)^2 + \lambda^2} + \frac{pk}{(p+k)^2 + \lambda^2} \\ &\quad + \frac{1}{2} \log \frac{(p-k)^2 + \lambda^2}{(p+k)^2 + \lambda^2}. \end{aligned} \quad (17)$$

C. A set of two non-linear equations.

At finite temperature $T \neq 0$ the mass gap equation for the quark running mass $m(p)$ couples to the one quark energy equation $E(p)$ through the Matsubara sum, and thus we get a system of three non-linear coupled equations,

$$\begin{aligned} m_T(p) &= m_0 + \frac{\sigma(T)}{p^3} \int_0^\infty \frac{dk}{2\pi} \mathcal{M}_T(k) \\ &\quad \frac{I_A(k, p, \lambda) m_T(k) p - I_B(k, p, \lambda) m_T(p) k}{\sqrt{k^2 + m_T(k)^2}}, \\ E_T(p) &= \frac{p^2 + m_0 m_T(p)}{\sqrt{p^2 + m_T(p)^2}} + \frac{\sigma(T)}{p^2} \int_0^\infty \frac{dk}{2\pi} \mathcal{M}_T(k) \\ &\quad \frac{I_A(k, p, \lambda) p k + I_B(k, p, \lambda) m_T(p) m_T(k)}{\sqrt{p^2 + m_T(p)^2} \sqrt{k^2 + m_T(k)^2}}, \end{aligned} \quad (18)$$

where the Matsubara sum normalized to 1 in the limit of small temperatures is,

$$\begin{aligned} \mathcal{M}_T(p) &= 2 \sum_{n=-\infty}^{+\infty} i k T \frac{i}{i(2n+1)\pi k T - [E(\mathbf{p}) - \mu]} \\ &= \tanh \frac{E_T(p) - \mu}{2kT}. \end{aligned} \quad (19)$$

To solve the coupled systems of non-linear Equations (18), we apply the techniques detailed in [4], *i. e.* we utilize a Padé ansatz for the quark running mass $m_T(p)$, we solve the mass gap variationally, we compute the one quark energy $E_T(p)$, we fit it with a Padé approximant, we feed it back into the mass gap equation, and then we repeat this cycle iteratively until the solution converges. The solution of the system of Eqs. (18) constitutes the main goal of this paper.

III. THE $T \neq 0$ SOLUTIONS OF THE MASS GAP EQUATION

Finite temperature T changes the mass gap equation in two different ways, in the temperature dependence of the string tension $\sigma(T)$ and in the Matsubara sum replacing the p^0 integral of the propagators. Since the finite temperature mass gap equation is numerically cumbersome to address, we first study separately the effect of each of these changes, before including both in the mass gap equation.

Note that we work in units of $\sqrt{\sigma} = \sqrt{0.19}$ GeV, the string tension commonly used in the Charmonium spectroscopy. For the transition temperature, we utilize the result computed in Lattice QCD [2, 3] of 0.176 (7) GeV. Thus we get $T_c = 0.40\sqrt{\sigma}$.

A. The effect of the finite temperature string tension $\sigma(T)$

Here we consider the T dependence of the string tension only. Notice this approach is exact when our infrared regulator $U_0 \rightarrow \infty$ as in the standard regularization of the linear potential of Eq. (12). In that case $E_T(p) \rightarrow \infty$ and the Matsubara sum $\mathcal{M}_T = 1$ is simply the same one occurring at $T = 0$.

Then the finite T mass gap equation is similar to $T = 0$ mass gap equation, just with a substitution of σ_0 by $\sigma(T)$. The mass gap solution can be found with a simple rescaling of the string tension.

In units of $\sqrt{\sigma} = 1$, we can fit the mass gap at the origin $m(0)$ as a function of the running mass m_0 with a function interpolating from the chiral limit constant to the massive case linear function with a simple irrational ansatz,

$$m(0) = \frac{a + m_0 + \sqrt{(a - m_0)^2 + 4b^2}}{2} \quad (20)$$

as depicted in Fig. (3 - left). Our fit produces $a = -2.29223\sqrt{\sigma}$, $b = 0.656306\sqrt{\sigma}$. Then our solution is simply found rescaling $\sqrt{\sigma}$ from 1 to $\sqrt{\sigma(T)}$

Our results, depicted in Figs. 7 and 8, show a chiral crossover, since the mass gap never vanishes due to the finite current quark mass m_0 . We observe in our results that the heavier the quark, the weaker the chiral crossover gets, as show in Figs. 7 and 8. For the

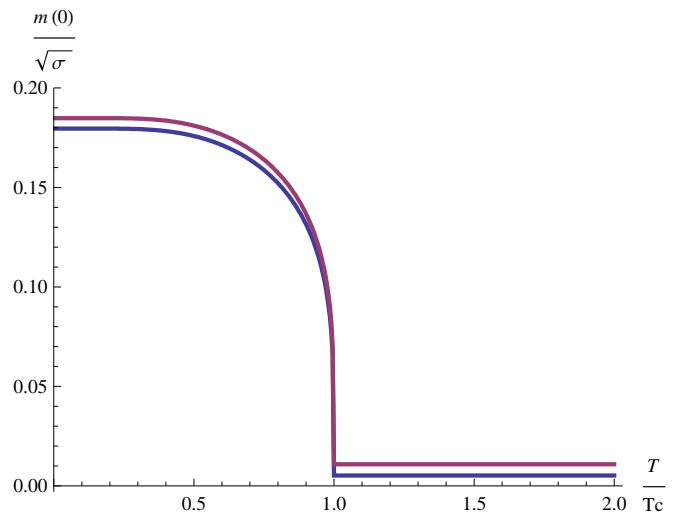


FIG. 7: Here we consider only the effect of the temperature in the string tension $\sigma(T)$, and plot the mass gap $m(0)$ as a function of T for the light u (lightest) and d (slightly heavier) quarks. We have a crossover, close to a phase transition since the current masses of the light quarks are much smaller than the dynamically generated constituent quark mass.

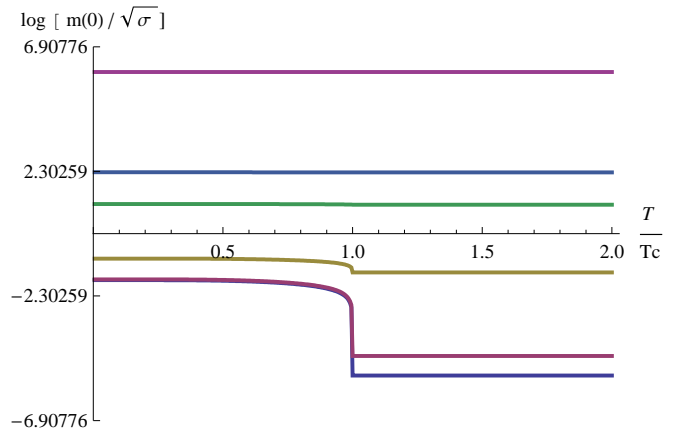


FIG. 8: Log plot of the mass gap $m_q(0)$, considering T effects in $\sigma(T)$ only, for the six different flavours of quarks as a function of T . From bottom to top we show the quarks u , d , s , c , b and t . The heavier the quark, the weaker the crossover gets.

heavier quarks the chiral crossover is very weak. On the other side, of light u and d quark masses, we still have a crossover since the mass gap starts finite at $T = 0$ and continues to be finite beyond T_c , although at large $T \gg T_c$ the mass gap is quite smaller than at vanishing T .

Notice that the mass gap $m(0)$ changes quite abruptly when T crosses T_c . The steepness of the light quark mass at $T = T_c$ is due to our fit of $\sigma(T)$ which is second-order like, as in Fig. 2. Possibly with a crossover-like $\sigma(T)$ reflecting the dynamical fermion effects, the crossover in

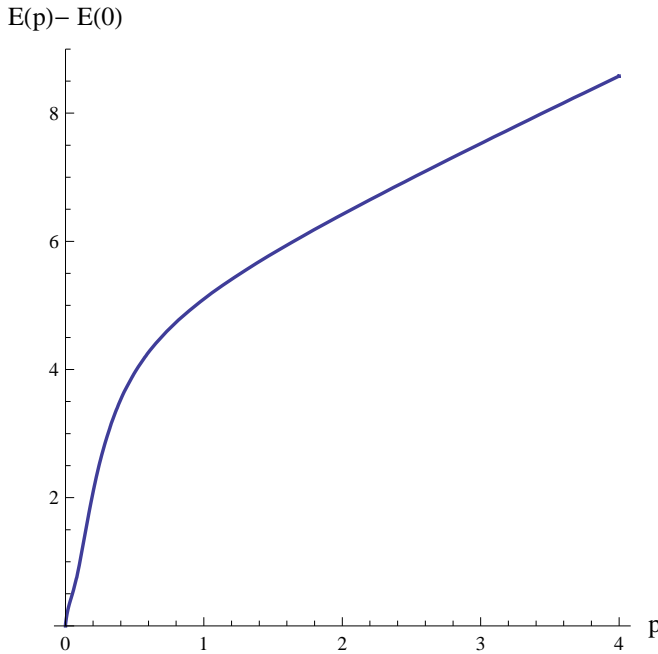


FIG. 9: A possible scenario to compute the Matsubara sum consists in using the one quark dispersion relation subtracted by the energy at the origin $E(p) - E(0)$. This produces the smallest possible quark energy to be used in the Matsubara sum. The other opposite scenario consists in utilizing the energy $E(p)$, with an infrared divergence of $\frac{\sigma}{2\lambda}$. In any case the one quark energy

the quark mass $m(0)$ may get slightly smoother. However we do not know exactly what happens at the transition temperature for light quarks, since an opposite effect can make the string tension steeper again at T_c . Indeed for light quarks one may argue that the internal energy U_1 (steeper than the free energy F_1) should be used. Thus in this paper we cannot address in detail the exact temperature where T crosses T_c , but rather the remaining range of temperatures.

B. The effect of the Matsubara sum effect in the propagator

Here we are interested in finding the effect of the Matsubara sum in the mass gap equation. To isolate this effect, we neglect any effect of the temperature T on the string tension, considering the string tension σ_0 at all temperatures.

We must then choose an infrared regulator, since adding a constant term $-U_0$ to the potential, say $-\sigma/\lambda$ as in Eq. (12), affects the energy which is then shifted $E_T(p) \rightarrow E_T(p) + U_0/2$. Thus at finite T , the solution of the system of Eqs. (18) depends on a constant shift of the potential, in contradistinction with vanishing temperature where $\mathcal{M}_T(p) \simeq 1$ decouples the energy $E_T(p)$ from the mass [4]. At finite T the one quark energy $E_T(p)$ con-

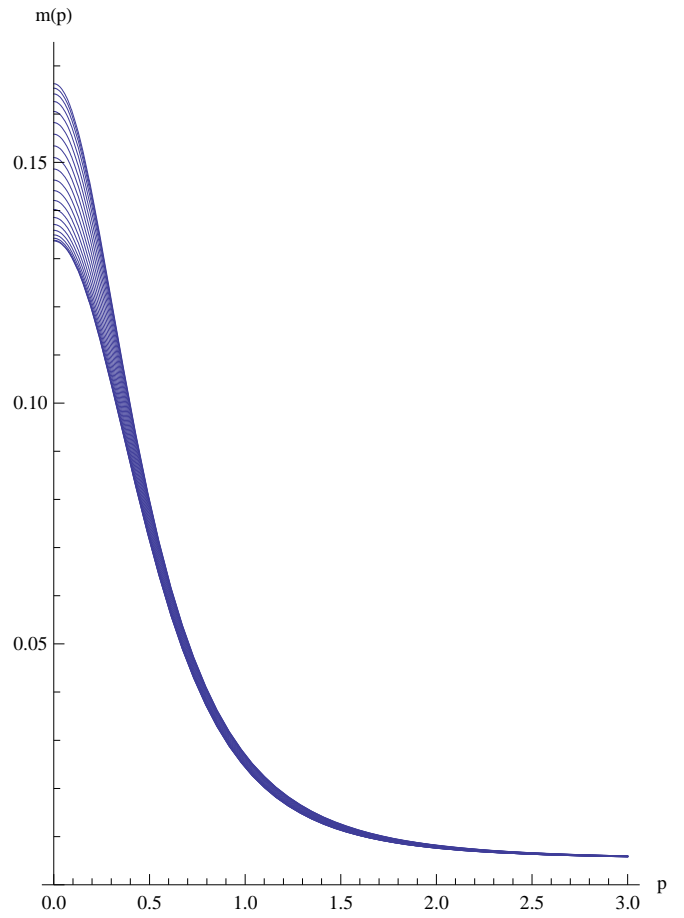


FIG. 10: Here we ignore the effect of the temperature in the string tension and consider only the effect of the Matsubara sum \mathcal{M}_T . We plot the running mass for the d quark, $m_d(p)$, computed for the different temperatures present in Table I, ranging from $T = 0$ to $T = T_c$. Note that the temperature decreases the quark mass, but the effect is much weaker than the string tension effect in Fig. 7.

tributes non-linearly to the Matsubara sum $D_T(p)$, and any change in $E_T(p)$ does change the solution of the mass gap and energy coupled equations and thus the three Eqs. (18) are coupled.

Here we choose a minimal U_0 , closer to the regularization of the linear potential of Eq. (14), just sufficient to cancel the one quark energy at vanishing momentum $E_T(0) = 0$. This case is also equivalent to the one when a chemical potential $\mu = E_T(0)$ is included, and thus $E_T(0) - \mu = 0$. We consider this case since it produces the largest possible effect in the Matsubara sum $D_T(p)$, interpolating between 0 at vanishing momentum and 1 at large momentum. This does suppress the infrared part of the integral if the mass gap equation up to $E_T(k) - E_T(0) \simeq kT$.

To exactly cancel the infrared divergences in the integrals, we utilize ansätze for the quark mass $m_T(p)$ and for the quark energy $E_T(p)$. Our numerical technique

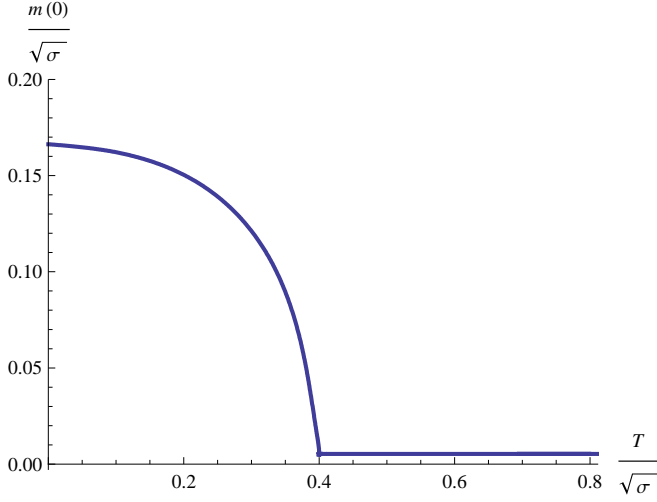


FIG. 11: Full computation of the mass gap for the d quark, $m_d(0)$, in the infrared regulator case where the Matsubara sum effects are maximal. Although not as steep close to $T = T_c$, the curve is quite similar to the one where we ignore the Matsubara sum effects. Again we have a crossover at T_c .

was tested in great detail for $T = 0$ and here we utilize the same ansatz and numerical techniques [4]. Our ansatz for $m_T(p)$ and $E_T(p)$ are the Padé approximants,

$$\begin{aligned} m_T(p) &= \frac{1}{c_0 + c_2 p^2 + c_4 p^4}, \\ E_T(p) &= \frac{\sigma}{2\lambda} - \frac{2\sigma}{\pi} \frac{p}{p^2 - m_T(p)^2} \\ &\quad + pC(p) + m_0 S(p) + \tilde{E}_T(p), \\ \tilde{E}_T(p) &= -\frac{1}{e_0 + e_1 p + e_3 p^3 + e_5 p^5}. \end{aligned}$$

After each iteration the resulting $m_T(p)$ and E_T are fitted again with our Padé approximants, and a new iteration is started. But for the solution for each temperature and mass is completely determined by the three parameters for the fits of $m_T(p)$, since $E_T(p)$ is a function of the quark mass.

To ensure convergence, we utilize the technique [4] of translating the mass gap equation into the variational equation for the vacuum energy density,

$$\begin{aligned} \mathcal{E} &= \frac{-g}{2\pi} \int_0^\infty \frac{dp}{2\pi} D_T(p) \left\{ 2p^3 C(p) + 2p^2 m_0 S(p) \right. \\ &\quad + \sigma(T) \int_0^\infty \frac{dk}{2\pi} D_T(k) \left[I_A(k, p, \mu) S(k) S(p) \right. \\ &\quad \left. \left. + I_B(k, p, \mu) C(p) C(k) \right] \right\}, \quad (21) \end{aligned}$$

now with a new dependence on temperature in σ_T (momentarily we consider $\sigma_T = \sigma_0$) and in the Matsubara sum \mathcal{M}_T . When the current mass is small compared

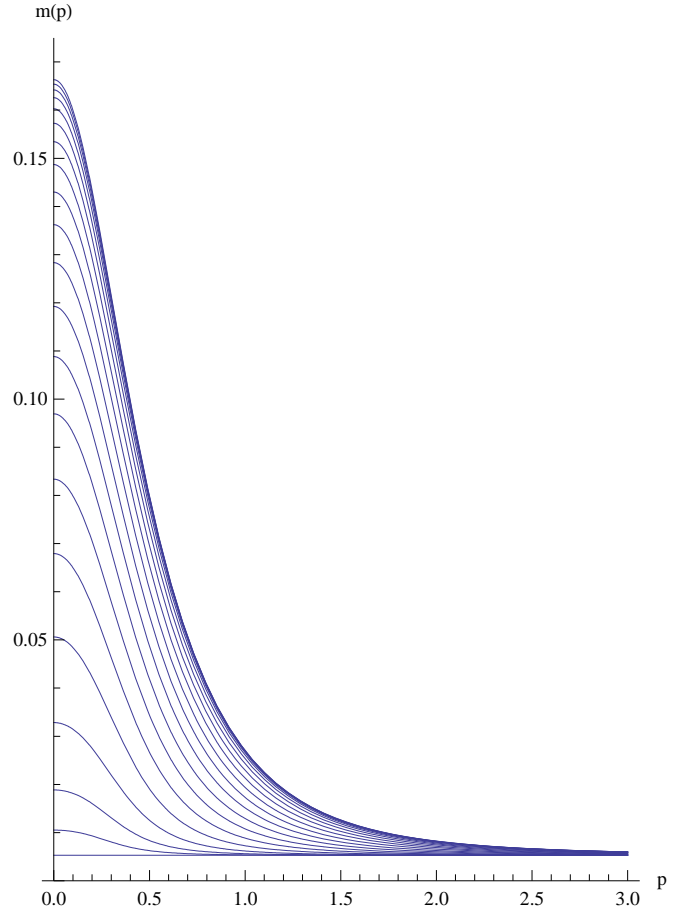


FIG. 12: Full computation of the running mass for the d quark, $m_d(p)$, computed for the different temperatures present in Table I, ranging from $T = 0$ to $T = T_c$. Unlike when the Matsubara sum only is considered, here the quark mass indeed equals the current quark mass M_d , almost vanishing, for $T = T_c$.

with the typical scale $\sqrt{\sigma(T)}$ of our problem, we utilize directly this equation. In the opposite case where the string tension is much smaller than the current mass, close to T_c , then the solution $m(p)$ is close to the current mass m_0 ,

$$m(p) \simeq m_0 + \frac{\sigma}{m_0} \mathcal{F}\left(\frac{p}{m_0}\right), \quad (22)$$

and then we only need to compute the dimensionless function $\mathcal{F}(p)$, produced perturbatively [4] after few iterations of the fixed point equation.

We consider the case of $m_0 = m_d$ corresponding to a d quark. Our results are illustrated in Fig. 10. Note that the effect of the Matsubara sum \mathcal{M}_T is to decrease the quark mass with increasing temperature, but nevertheless the Matsubara sum effect in Fig. 10 is much weaker than the string tension effect shown in Fig. 7.

m_0	T	$10^4 \frac{\varepsilon - \varepsilon_0}{g}$	c_0	c_2	c_4
0.00527656	0.000000	-0.558232	6.20966	25.2077	14.5339
0.00527656	0.0313837	-0.514877	6.24603	25.1480	14.6870
0.00527656	0.0625738	-0.482888	6.29268	25.0808	14.8787
0.00527656	0.0933782	-0.456189	6.35722	25.0130	15.1468
0.00527656	0.123607	-0.425455	6.45135	25.0128	15.5903
0.00527656	0.153073	-0.390516	6.57955	25.2058	16.3132
0.00527656	0.181596	-0.35179	6.74966	25.6934	17.4403
0.00527656	0.208999	-0.309921	6.97245	26.5531	19.1262
0.00527656	0.235114	-0.265958	7.26188	27.8649	21.5887
0.00527656	0.259779	-0.221304	7.63714	29.7358	25.1689
0.00527656	0.282843	-0.177546	8.12658	32.3267	30.4365
0.00527656	0.304162	-0.136292	8.77490	35.8925	38.3987
0.00527656	0.323607	-0.0990367	9.65716	40.8552	50.9525
0.00527656	0.341056	-0.0670518	10.9094	47.9602	71.9645
0.00527656	0.356403	-0.0412995	12.8039	58.6492	110.150
0.00527656	0.369552	-0.0223216	15.9619	76.1081	187.827
0.00527656	0.380423	-0.0100832	22.0570	108.769	371.573
0.00527656	0.388948	-0.00365887	36.2780	183.098	886.265
0.00527656	0.395075	-0.00105524	73.6460	382.799	2491.37
0.00527656	0.398767	-0.000187953	190.883	1073.65	9021.24
0.00527656	0.400000	-0.0000000	∞	∞	∞

TABLE I: The parameters for the quark functions $m_T(p)$ defined in Eq. (21).

C. Full solution of the mass gap equation at finite temperature T

Here we determine the full solution of the mass gap equation at finite temperature T , utilizing Eq. (21), but combining the temperature effects in the string tension $\sigma(T)$ with the temperature effects in the Matsubara sum $\mathcal{M}_T(p)$. In the present case we continue to consider that $\mu = E(0)$, the case maximizing the finite temperature effects of the Matsubara sum.

We now fix the current quark mass to $m_0 = m_d$, quark d current mass and run the temperature T so that we get a curve. We numerically consider a set of temperatures denser at T_c , with the parametrization of $T = T_c \cos \theta$ where the θ considered are equally spaced in the interval ranging between $\pi/2$ and 0. We show the best fitting parameters c_0, c_2, c_4 , in Table I, we depict the mass gap

critical curve in Fig. 11 and we show the different running quark masses in Fig. 12. It occurs that indeed a crossover is found in the mass gap critical curve at $T = T_c$, and that the critical curve is similar (but not identical) to the critical curve computed with the string tension temperature effects only.

IV. CONCLUSION

We apply a new variational technique, in the framework of a CG χ QM, to solve the mass gap equation at finite temperature T . The quark mass $m_T(p)$ and the quark energy $E_T(p)$ are fitted with Pad approximants, the quark mass parameters are displayed in Table I.

We compare the two different temperature contributions, in the string tension $\sigma(T)$ and in the Matsubara sum $\mathcal{M}_T(p)$. It occurs that the dominant contribution, and also the simplest one to apply in the quark model, is the one of the string tension $\sigma(T)$. This happens not only because the deconfinement critical temperature $T_c = 0.40\sqrt{\sigma}$ is relatively small when compared to the string tension at vanishing temperature σ_0 , but also because the Matsubara sum never vanishes while the string tension really vanishes when $T \rightarrow T_c$. Thus the quark mass critical curve has a shape similar to the string tension critical curve, but the curves are not exactly identical since the quark critical curve is less steep at $T \simeq T_c$.

Moreover, since the light current quark masses m_u and m_d are small compared with the string tension at vanishing temperature σ_0 , the quark mass gap $m(0)$ essentially follows the string tension curve. This is a quite simple result, relevant for further studies at finite temperature.

With our excellent fits of the dynamical quark mass $m_T(p)$ and of the quark dispersion relation $E_T(p)$ we are now well equipped to address further studies, such as the hadronic excited spectra at finite temperature T .

Acknowledgments

I am very grateful to Marlene Nahrgang, to Pedro Sacramento and to Jan Pawłowski for discussions on the QCD phase diagram motivating this paper. I acknowledge the financial support of the FCT grants CFTP, CERN/FP/109327/2009 and CERN/FP/109307/2009.

[1] CBM Progress Report, publicly available at <http://www.gsi.de/fair/experiments/CBM/>, (2009).
[2] Y. Aoki, G. Endrodi, Z. Fodor, S. D. Katz and K. K. Szabo, Nature **443**, 675 (2006) [arXiv:hep-lat/0611014].
[3] Y. Aoki, Z. Fodor, S. D. Katz and K. K. Szabo, Phys. Lett. B **643**, 46 (2006) [arXiv:hep-lat/0609068].
[4] P. Bicudo, to be published in Nuc. Phys. A, (2011), doi:10.1016/j.nuclphysa.2011.09.014, [arXiv:1007.2044

[hep-ph]].
[5] P. Bicudo, M. Cardoso, T. Van Cauteren and F. J. Llanes-Estrada, Phys. Rev. Lett. **103**, 092003 (2009) [arXiv:0902.3613 [hep-ph]].
[6] P. Bicudo, Phys. Rev. D **81**, 014011 (2010) [arXiv:0904.0030 [hep-ph]].
[7] P. Bicudo, Phys. Rev. Lett. **72**, 1600 (1994).
[8] O. A. Battistel and G. Krein, Mod. Phys. Lett. A **18**,

- 2255 (2003).
- [9] S. M. Antunes, G. Krein, V. E. Vizcarra and P. K. Panda, *Braz. J. Phys.* **35**, 877 (2005).
 - [10] L. Y. Glozman and R. F. Wagenbrunn, *Phys. Rev. D* **77**, 054027 (2008) [arXiv:0709.3080 [hep-ph]].
 - [11] P. Guo and A. P. Szczepaniak, *Phys. Rev. D* **79**, 116006 (2009) [arXiv:0902.1316 [hep-ph]].
 - [12] P. M. Lo and E. S. Swanson, arXiv:0908.4099 [hep-ph].
 - [13] T. Kojo, Y. Hidaka, L. McLerran and R. D. Pisarski, arXiv:0912.3800 [hep-ph].
 - [14] A. V. Nefediev and J. E. F. Ribeiro, arXiv:0906.1288 [hep-ph].
 - [15] P. Bicudo, *Phys. Rev. D* **79**, 094030 (2009) [arXiv:0811.0407 [hep-ph]].
 - [16] O. Kaczmarek, F. Karsch, E. Laermann and M. Lutgemeier, *Phys. Rev. D* **62**, 034021 (2000) [arXiv:hep-lat/9908010].
 - [17] M. Doring, K. Hubner, O. Kaczmarek and F. Karsch, *Phys. Rev. D* **75**, 054504 (2007) [arXiv:hep-lat/0702009].
 - [18] K. Hubner, F. Karsch, O. Kaczmarek and O. Vogt, *Phys. Rev. D* **77**, 074504 (2008) [arXiv:0710.5147 [hep-lat]].
 - [19] O. Kaczmarek and F. Zantow, *Phys. Rev. D* **71**, 114510 (2005) [arXiv:hep-lat/0503017].
 - [20] O. Kaczmarek and F. Zantow, arXiv:hep-lat/0506019.
 - [21] O. Kaczmarek and F. Zantow, *PoS LAT2005*, 192 (2006) [arXiv:hep-lat/0510094].
 - [22] P. Bicudo, *Phys. Rev. D* **82**, 034507 (2010) [arXiv:1003.0936 [hep-lat]].
 - [23] R. Feynman, R. Leighton, M. Sands, "The Feynman Lectures on Physics", Vol II, chap. 36 "Ferromagnetism", published by Addison Wesley Publishing Company, Reading, Massachusetts, ISBN 0-201-02117-x (1964).
 - [24] T.D. Lee, *Particle Physics and Introduction to Field Theory*, (Harwood Academic Publishers, New York, 1981).
 - [25] A. Szczepaniak, E. S. Swanson, C. R. Ji and S. R. Cotanch, *Phys. Rev. Lett.* **76**, 2011 (1996) [arXiv:hep-ph/9511422].
 - [26] A. P. Szczepaniak and E. S. Swanson, *Phys. Rev. D* **55**, 1578 (1997) [arXiv:hep-ph/9609525].
 - [27] I. I. Balitsky, *Nucl. Phys. B* **254**, 166 (1985).
 - [28] H. G. Dosch, *Phys. Lett. B* **190**, 177 (1987).
 - [29] H. G. Dosch and Yu. A. Simonov, *Phys. Lett. B* **205**, 339 (1988).
 - [30] P. Bicudo, N. Brambilla, E. Ribeiro and A. Vairo, *Phys. Lett. B* **442**, 349 (1998) [arXiv:hep-ph/9807460].
 - [31] A. Le Yaouanc, L. Oliver, O. Pene, J. C. Raynal, *Phys. Lett.* **134B**, 249 (1984).
 - [32] A. Amer, A. Le Yaouanc, L. Oliver, O. Pene and J.-C. Raynal, *Phys. Rev. Lett.* **50**, 87 (1983).
 - [33] A. Le Yaouanc, L. Oliver, O. Pene and J.-C. Raynal, *Phys. Rev. D* **29**, 1233 (1984);
 - [34] A. Le Yaouanc, L. Oliver, S. Ono, O. Pène and J. C. Raynal, *Phys. Rev. D* **31**, 137 (1985).
 - [35] Y. L. Kalinovsky, L. Kaschluhn and V. N. Pervushin, *Phys. Lett. B* **231**, 288 (1989).
 - [36] P. Bicudo, J. E. Ribeiro, *Phys. Rev. D* **42**, 1611 (1990); *Phys. Rev. D* **42**, 1625 (1990); *Phys. Rev. D* **42**, 1635 (1990).
 - [37] S. L. Adler, A. C. Davis, *Nucl. Phys. B* **244**, 469 (1984),
 - [38] P. Bicudo, J. E. Ribeiro and J. Rodrigues, *Phys. Rev. C* **52**, 2144 (1995).
 - [39] R. Horvat, D. Kekez, D. Palle and D. Klabucar, *Z. Phys. C* **68**, 303 (1995).
 - [40] F. J. Llanes-Estrada, S. R. Cotanch, *Phys. Rev. Lett.* **84**, 1102 (2000).
 - [41] R. F. Wagenbrunn and L. Y. Glozman, *Phys. Rev. D* **75**, 036007 (2007) [arXiv:hep-ph/0701039].